Microchimica Acta (2022) 189: 341
https://doi.org/10.1007/s00604-022-05434-y

ORIGINAL PAPER

# Electrochemical determination of acetamiprid using PEDOT sensing coating functionalized with carbon quantum dots and Prussian blue nanoparticles

**Shuqi Shang[1] · Dongwei Wang[1] · Jiasheng Wang[1]**

Received: 14 March 2022 / Accepted: 26 July 2022 / Published online: 23 August 2022


**Abstract**
A dual-mode electrochemical biosensor for acetamiprid detection was proposed for the first time based on carbon quantum dots/Prussian blue (CQDs/PB)-functionalized poly(3,4-ethylenedioxythiphene) (PEDOT) nanocomposite. The nanocomposite with spherical stacking nanostructure showed high surface area, excellent catalytic ability, and cycling stability. The biosensor can be effortlessly constructed after the immobilization of acetamiprid aptamer. The concentration of acetamiprid can be determined by differential pulse voltammetry (DPV) based on its signal change deduced from the pristine PB. With the capture of acetamiprid, the response current (I-T) signal generated by hydrogen peroxide catalysis from the biosensor can also been used to establish the method for monitoring acetamiprid. The dual-mode biosensor showed a wide linear range from $10^{-12}$ g $mL^{-1}$ to $10^{-6}$ g $mL^{-1}$, low detection limits of $6.84 \times 10^{-13}$ g $mL^{-1}$ and $4.99 \times 10^{-13}$ g $mL^{-1}$, and ultrafast detection time of 25 s and 5 s through DPV and I-T mode, respectively. The biosensor possessed excellent selectivity and stability. More importantly, the biosensor was successfully applied to detect acetamiprid residues in vegetables, proving a promising approach for routine detection of pesticide in real samples.

**Keywords** Dual-mode · Carbon quantum dots · Prussian blue · Conducting polymer · Biosensor · Differential pulse voltammetry · Acetamiprid

## Introduction

The accumulation of acetamiprid (ATP) poses a threat to environmental security, food safety, and human health [1]. Thus, the development of a simple, sensitive, selective, and field-portable acetamiprid detection strategy is still imminent. Many analytical methods have been applied for the detection of acetamiprid, mainly including gas chromatography [2], high-performance liquid chromatography [3], and liquid/gas chromatography coupled with mass spectrometry [4]. Conventional techniques for pesticide detection are limited by the disadvantages of time-consuming, skilled manpower, high cost, and harsh operating conditions [5]. Different from those methods based on large instruments, the electrochemical biosensors provide a promising analytical alternative for pesticide analysis and gain significant attention due to their unique advantages, such as the rapid response time, the low limit of detection, the cost-effectiveness, and ease to operate [6].

To improve the sensitivity and stability of the analysis, a variety of nanomaterials were successfully used to construct the biosensors for the assay of pesticide residue, including carbon-based nanomaterials and conducting polymers as well as nanocomposites in the form of nanoparticles, nanowires, or porous nanostructures [7, 8]. Conducting polymers, such as polyaniline, polypyrrole, and polythiophene, have been extensively investigated as biosensor substrate for their enormous functionalization potential and favorable electrochemical functions [9]. For instance, poly(3,4-ethylenedioxythiophene) (PEDOT) was reported as a new electrochemical active material to construct the enzyme-based biosensor for the assay of organophosphate insecticides, which acted not only as a conductive formwork but also as an electrochemical mediator for thiocholine oxidation [10]. The combination of carbon-based material with the conducting

Shuqi Shang and Dongwei Wang contributed equally to this work.

✉ Jiasheng Wang
jiasheng0813@163.com

[1] College of Mechanical and Electrical Engineering, Qingdao Agricultural University, Qingdao 266109, China

polymer has attracted much attention due to the synergistic effect in the electronic property.

In the large family of carbon-based materials, carbon quantum dots (CQDs), as a fascinating class of zero-dimensional (0-D) carbon nanomaterials, have been applied in the fields of biological imaging, clinical diagnostics, biosensors, and catalysts due to their advantages such as high chemical stability, good biocompatibility, high hydrophilicity, and mass production at low cost [11]. Carboxyl-functionalized CQDs with high solubility in aqueous solution are beneficial to the immobilization of a large number of biomolecules. The properties of carbon composites as sensing interface can be significantly improved after the modification with Prussian blue (PB) [12].

PB, a classical prototype of transition metal hexacyanometalates, has been widely studied due to its unique reversible redox activity, catalytic property, good biocompatibility, and easy preparation [13]. And PB-based sensing platforms have been used for the assay of hydrogen peroxide, L-cysteine, and protein [10, 14, 15]. However, consideration of its special limited stability, gradual decrease of catalytic activity, and low Coulomb efficiency, the application of PB in the field of sensing and energy storage has been greatly constrained. It is an effective strategy to solve this issue that PB forms the composites with various nanomaterials, including the conducting polymer, carbon nanotube, graphene, graphene oxide, and graphene quantum dots [14, 16–18]. So far, the preparation and application of CQDs/PB nanocomposites have received little attention.

Since the single-mode detection method may easily lead to no ability of self-verification of the results and poor anti-interference capacity, the dual-mode biosensors have shown much higher effectiveness and reliability using two different principles and relatively independent signal output [19]. In this work, we proposed an electrochemical dual-mode biosensor for ultrasensitive and ultratrace detection of acetamiprid based on the PEDOT/CQDs/PB nanoparticles. CQDs/PB hybrid was firstly prepared through PB anchored on carboxylated CQDs by a spontaneous redox reaction between $FeSO_4$ and $K_3[Fe(CN)]_6$. Subsequently, CQDs/PB acted as "template" to guide the formation of PEDOT/CQDs/PB nanoparticles. Integrating the reversible redox activity of PB and good biocompatibility of CQDs with the favorable electrochemical properties of PEDOT, the prepared PEDOT/CQDs/PB nanoparticles can provide a good substrate for the immobilization of acetamiprid aptamer to construct the novel dual-mode biosensor (Scheme 1).

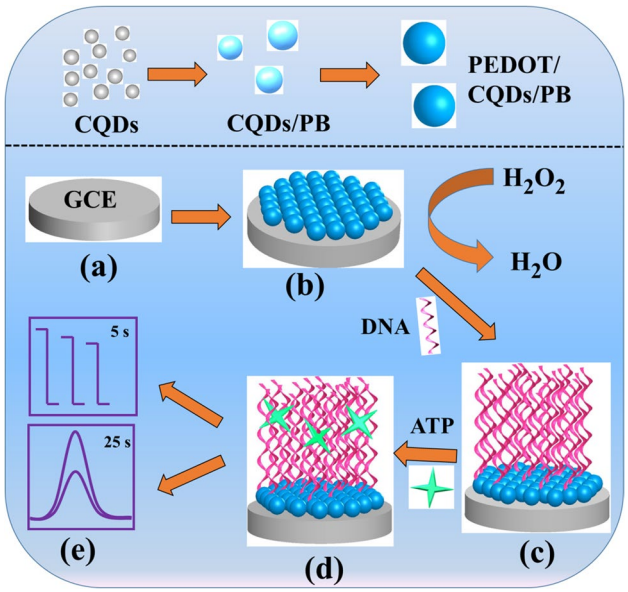


**Scheme 1** The working principle of dual-mode biosensor based on PEDOT/CQDs/PB. (a) The bare GCE; (b) PEDOT/CQDs/PB/GCE; (c) DNA/PEDOT/CQDs/PB/GCE; (d) ATP/DNA/PEDOT/CQDs/PB/GCE; (e) the dual-mode output

## Experimental section

### Reagents and apparatus

$H_2O_2$ (30%) and $KMnO_4$ were bought from Laiyang Kangde Chemical Co., Ltd. EDOT, acetamiprid, methyl parathion, chlorpyrifos, and fenitrothion were obtained from Aladdin regent (Shanghai, China). Acetamiprid aptamer (ctg aca cca tat gaa ga) was obtained from Shanghai Bioengineering Co., Ltd (Shanghai, China).

For all electrochemical measurements, field emission scanning electron microscope (SEM) of the modified electrodes, Fourier transform infrared (FTIR), X-ray photoelectron spectroscopy (XPS), X-ray diffraction (XRD) analysis, and high-performance liquid chromatography (HPLC), the required instruments and components, are listed in the supporting materials.

### The synthesis of nanomaterial

#### The synthesis of CQDs and CQDs/PB

According to the previous report, the carboxylated CQDs were synthesized successfully [20]. The preparation process of CQDs and CQDs/PB was described in the supporting material.

#### The synthesis of PEDOT/CQDs/PB

Ten-milligram CQDs/PB composite was dissolved in 5 ml deionized water under the ultrasonic condition. Ten-microliter EDOT was subsequently dropped and ultrasonically treated until it was completely dissolved to obtain the deposition solution. The PEDOT/CQDs/PB composites were deposited onto glassy carbon electrode (GCE) using

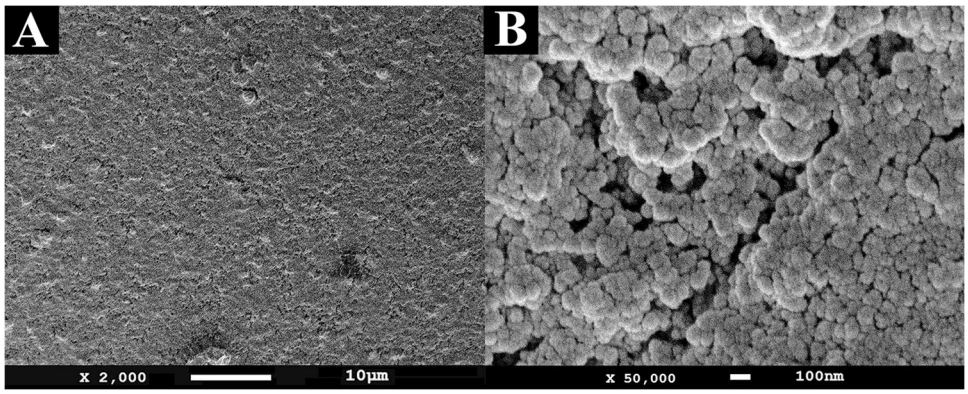


**Fig. 1** SEM images of PEDOT/CQDs/PB at low and high magnifications

cyclic voltammetry (CV) technique with the potential range from – 0.2 V to 1.2 V and 15 cycles (Figure S1). The modified electrode was defined as PEDOT/CQDs/PB/GCE.

### The electrochemical sensing of hydrogen peroxide on PEDOT/CQDs/PB

The catalytic ability of the PEDOT/CQDs/PB composite for hydrogen peroxide was investigated using the CV and I-T techniques. The specific parameters are listed in the supporting material.

### The dual-mode assay of acetamiprid

PEDOT/CQDs/PB/GCE was immersed in PBS (pH 7.4, 0.2 M) containing 0.4 M EDC, 0.1 M NHS, and $10^{-6}$ M acetamiprid aptamer for 1.0 h, and then it was washed with water and PBS three times, respectively. The aptasensor (DNA/PEDOT/CQDs/PB/GCE) was obtained. After DNA/PEDOT/CQDs/PB/GCE was incubated in different concentrations of acetamiprid, DPV was recorded in 5.0 mL PBS (pH 4.0, 0.2 M). This was the first mode of acetamiprid detection. Meanwhile, with the capture of acetamiprid, the catalytic ability of the biosensor for hydrogen peroxide was also weakened, and the catalytic current of the same amount of hydrogen peroxide shown on the I-T curve was also reduced, which was the second mode of acetamiprid detection (Scheme 1).

### Preparation and determination of the real sample

Fresh cabbage was cultivated in our laboratory. Cabbage samples were pretreated as follows. The cabbages were washed and dried for standby. Cabbages (10 g) were added to the system containing 5 mL of water and 20 mL of acetonitrile. The mixture was ultrasonicated for 30 min and filtrated. The obtained filtrate was centrifuged at 4000 rpm for 15 min, and the acetonitrile in the supernatant was rotatably evaporated at 55 °C; then, the concentrated solution was obtained. Finally, the concentrated sample was diluted 100-fold with PBS (pH 7.4) for the following acetamiprid detection.

For the acetamiprid analysis in the diluted cabbage extract, various amount of acetamiprid (with the final concentrations of 0, $10^{-12}$, $10^{-11}$, $10^{-10}$, $10^{-9}$, $10^{-8}$, $10^{-7}$, and $10^{-6}$ g $mL^{-1}$) were dropped into the obtained matrix of the diluted cabbage samples. The DPVs were recorded in 5.0 mL PBS (pH 4.0, 0.2 M).

## Results and discussion

### The characteristics of the nanocomposites

The surface morphology of the CQDs, CQDs/PB, and PEDOT/CQDs/PB were characterized by SEM. Figure 1 showed that the PEDOT/CQDs/PB nanocomposite was uniformly stacked granules with an average particle diameter of 100 nm. CQDs/PB nanocomposite with a large amount of carboxyl groups was very soluble in water and negatively charged, which made it suitable to act as an excellent dopant for the polymerization of conducting polymers (Figure S2). Negatively charged dopants can balance the positively charged PEDOT backbone to ensure the successful development of polymerization, such as peptide, protein, multi-walled carbon nanotubes, and graphene oxide [21, 22]. Therefore, CQDs/PB nanocomposite acted as "templates" to guide the polymerization of PEDOT, protecting the CQDs/PB nanoparticle as a covering shell. PEDOT/CQDs/PB nanocomposite formed a uniform granular nanostructure and expanded the surface area of the modified electrode.

XPS measurement was used to study the composition of PEDOT/CQDs/PB and the successful immobilization of acetamiprid aptamer. As shown in Fig. 2A, the fully scanned spectra of PEDOT/CQDs/PB contained S 2p (163.97 eV), C 1 s (286.11 eV), N 1 s (409.4 eV), O 1 s (533 eV), and Fe 2p (708.4 eV), which illustrated that the conducting polymer

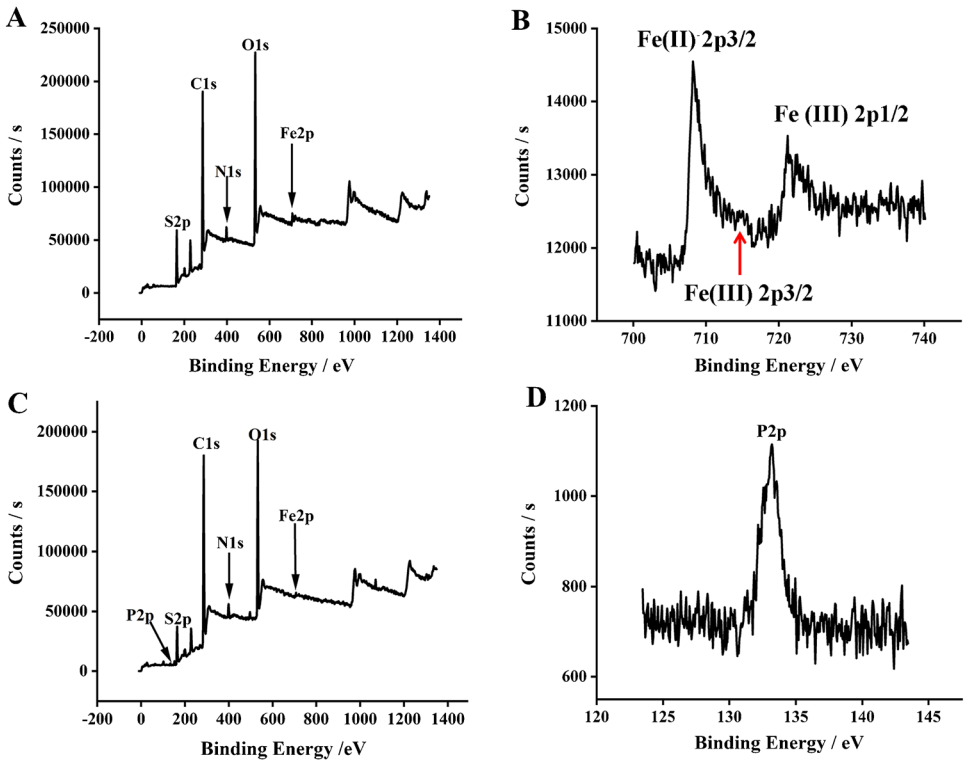


**Fig. 2** XPS survey spectra of the PEDOT/CQDs/PB (**A**) and DNA/PEDOT/CQDs/PB (**C**). High-resolution XPS spectra for Fe 2p (**B**) of the PEDOT/CQDs/PB and P 2p (**D**) of the DNA/PEDOT/CQDs/PB

PEDOT (the only source of S element) and CQDs/PB (the only source of Fe element) were successfully synthesized into an integral composite. Estimating from the Fe 2p pattern (Fig. 2B), it could be observed that three binding energy peaks of Fe $2p_{3/2}$ and Fe $2p_{1/2}$ were located at 708.2, 711.2, and 724.8 eV, which were corresponding to the presence of $[Fe(CN)_6]^{4-}$, $Fe^{3+}$, and PB nanoparticles, respectively [23]. Upon comparing the XPS pattern of PEDOT/CQDs/PB (Fig. 2A) and DNA/PEDOT/CQDs/PB (Fig. 2C and D), it could be found that after the immobilization of acetamiprid aptamer, new P 2p peak appeared with the decrease of S 2p and Fe 2p peaks, showing the successful attachment of aptamer. Table S1 shows the quantitative analysis of the modified surfaces.

The FTIR spectrum of CQDs (Figure S3A, curve a) showed strong features at 1593 $cm^{-1}$, 1361 $cm^{-1}$, and 1271 $cm^{-1}$ corresponding to the symmetric and antisymmetric stretches of C = O and C–O–C respectively, which was consistent with the presence of the carboxylate groups of CQDs [24]. For the FTIR spectrum of CQDs/PB (curve b), the new band appeared at 2084 $cm^{-1}$, which was ascribed to the stretching vibration peak of C≡N, proving that PB has successfully combined with CQDs as a whole. More interestingly, for the spectrum of PEDOT/CQDs/PB, the new appearance of the band at 1065 $cm^{-1}$ corresponded to the stretching vibration absorption peak of C-S, suggesting the successful preparation of PEDOT/CQDs/PB.

UV–vis spectral analysis was performed to verify the preparation of CQDs and CQDs/PB (Figure S3B). CQDs have been reported to display strong optical absorption in the UV and near-visible regions [24]. It was observed that CQDs aqueous solution had an obvious absorption peak at 322 nm (curve a). In addition, there was a strong absorption peak at 693 nm corresponding to PB [25] (curve b).

The XRD pattern of the CQDs (Figure S3C, curve a) also displayed a broad peak centered at 29.5° (2$\theta$), which was also attributed to the highly disordered carbon atom [26]. For the patterns of CQDs/PB and PEDOT/CQDs/PB, the diffraction peaks at 17.55°, 24.75°, 35.40°, and 39.00° (curves b and c) referred to the reflections of the face-centered-cubic phase of PB [14]. After the co-deposition of PEDOT and CQDs/PB, these patterns of the PB peaks did not change significantly.

## The catalytic property of hydrogen peroxide by PEDOT/CQDs/PB

As shown in Figure S4A, PEDOT/CQDs/PB/GCE displayed a pair of well-defined redox peaks, corresponding to the reversible transformation between PB and Prussian white [27]. With the addition of $H_2O_2$, the cathode peak/anode peak current of PEDOT/CQDs/PB/GCE increased (curve b), indicating that PEDOT/CQDs/PB

nanocomposite had good catalytic performance for $H_2O_2$. Figure S4B showed that the maximum response current to hydrogen peroxide was produced at 0 V. A typical amperometric I-T plot of PEDOT/CQDs/PB/GCE was studied by continuously adding $H_2O_2$ to PBS (pH 4.0) at 0.0 V (Figure S4C). The response current was linear with the $H_2O_2$ concentration ranging from 0.1 mM to 0.9 mM with a detection limit of 0.0287 mM (Figure S4D). More detailed discussions are listed in the supporting materials.

## Construction of a dual-mode acetamiprid aptasensor

As shown in Scheme 1, PEDOT/CQDs/PB was employed as an electrochemical sensing platform for the assay of acetamiprid. CV is a convenient and practical way to characterize the step-by-step preparation of modified electrodes. Figure 3A shows that the bare electrode had no peak in 0.2 M PBS (pH 4.0). Interestingly, after acetamiprid aptamer was immobilized onto the PEDOT/CQDs/PB-modified electrode, the well-defined redox peak current of PB decreased obviously. When acetamiprid was specifically captured by the biosensor, the aptamer-acetamiprid complex reduced the peak current of PB (curve d). These results indicated that PEDOT/CQDs/PB was an excellent electrochemical indicator. As shown in Fig. 3B, the DPV tests were also used to characterize the properties of the biosensors. Typically, the bare GCE showed a smooth straight line (curve a). The sequential immobilization of both acetamiprid aptamer and acetamiprid led to the corresponding decrease of the oxidation peak current of PB. Furthermore, Figure S5 shows that the electrochemical reaction on the biosensor was a diffusion-controlled process.

## The dual-mode aptasensor for the assay of acetamiprid

Figure S7 shows the best DPV parameter setting: the increased voltage was 0.1 V; the amplitude was 0.1 Hz; the pulse width was 0.06 s; and the pulse period was 0.5 s. The optimal detection pH was 4.0 and the optimal number of deposition cycle for PEDOT/CQDs/PB was 12 cycles.

Under the optimized experimental conditions, the biosensor was performed for the quantitative assay of acetamiprid. The peak current of DNA/PEDOT/CQDs/PB/GCE decreased with the increasing acetamiprid concentration (Fig. 4A). The signal inhibition rate ($\Delta I/I_0$) was in a linear relationship with the acetamiprid concentration within the range from $10^{-12}$ to $10^{-6}$ g mL$^{-1}$, where $I_0$ represents the signal value without acetamiprid, and $\Delta I$ is the current change. Linear fitting equation was $\Delta I/I_0 = 0.05779 \log C + 0.7087$ ($R^2 = 0.993$) (Fig. 4B) with the detection limit (LOD) of the method $6.84 \times 10^{-13}$ g mL$^{-1}$ ($S/N = 3$).

Incubation of acetamiprid with different concentrations on the biosensor may change its catalytic ability for $H_2O_2$, thus affecting the response current ($\Delta I$). The I-T method was used to determine the response current of the biosensor incubating different concentrations of acetamiprid towards $H_2O_2$ (0.1 mM), as shown in Fig. 4C. Figure 4D shows that the linear regression equation ($\Delta I = -0.1257\ C + 0.6075$, $R^2 = 0.994$) was obtained with the acetamiprid concentration within the range from $10^{-12}$ to $10^{-6}$ g mL$^{-1}$, and the LOD of the method was $4.99 \times 10^{-13}$ g mL$^{-1}$. The dual-mode excellent analytical performance of the biosensor for acetamiprid detection was compared with that of other biosensors previously reported in Table 1. The lower detection limit and the wider linear range may be attributed to the following reasons. Firstly, PEDOT/CQDs/PB can effectively integrate the merits of three components, with excellent electrical conductivity and its own electrochemical indicator. Secondly, spherical PEDOT/CQDs/PB with a large surface area had a large number of carboxyl groups for fixing the aptamers and provided a biocompatible environment to maintain the activity of the aptamers. Finally, the forceful and selective combination between aptamer and acetamiprid ensured the excellent sensing performance of the biosensor.

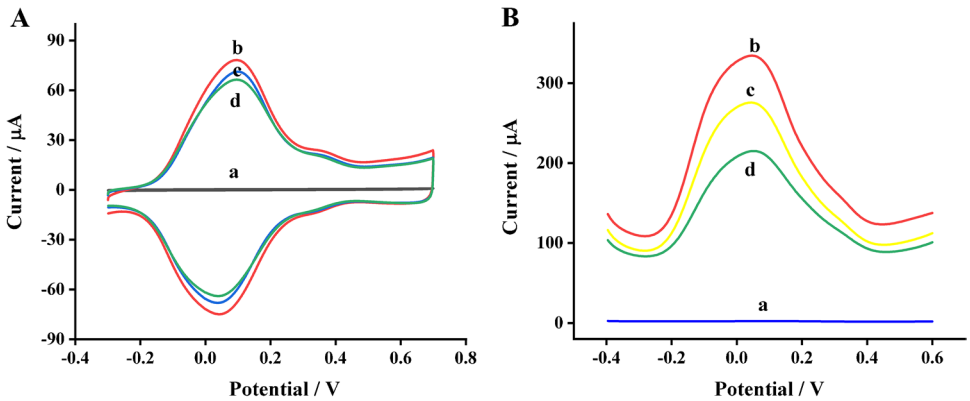


**Fig. 3** CV (**A**) and DPV (**B**) of the sensors recorded in 0.2 M PBS (pH 4.0). The curves represent the bare electrode (a), PEDOT/CQDs/PB/GCE (b), DNA/PEDOT/CQDs/PB/GCE (c), and ATP/DNA/PEDOT/CQDs/PB/GCE (d)

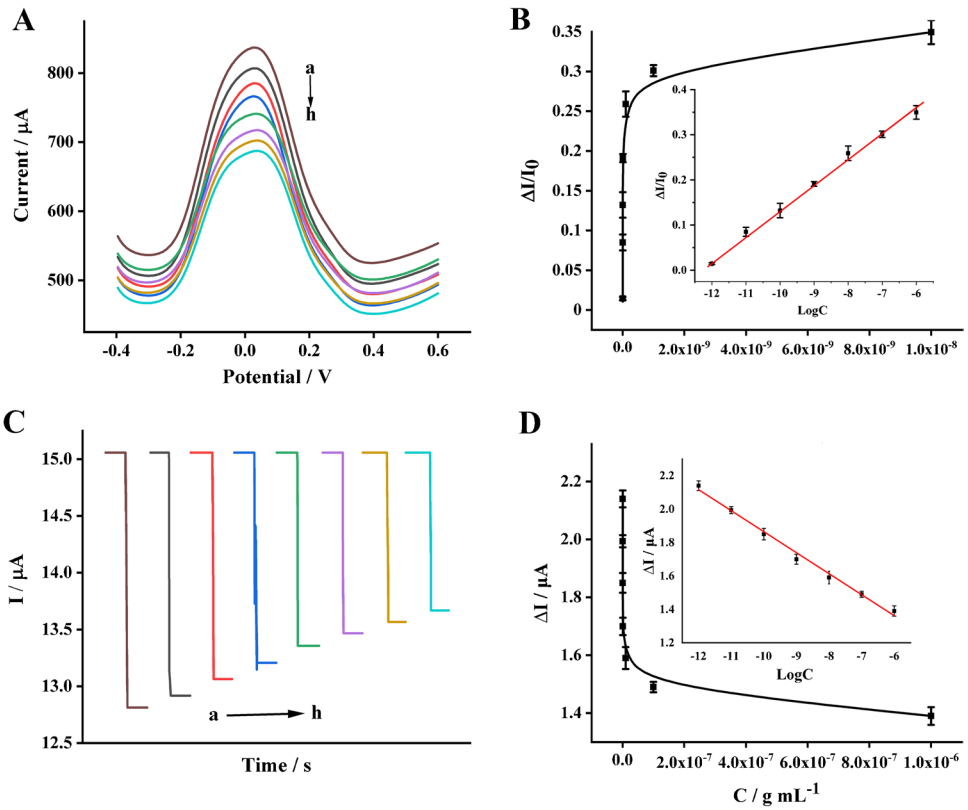


**Fig. 4** (**A**) DPV curves of the DNA/PEDOT/CQDs/PB/GCE towards different concentrations of acetamiprid; (**B**) the signal inhibition rate ($\Delta I/I_0$) of the biosensor after incubation with different concentrations of acetamiprid. The inner illustration showed the linear relationship between the logarithm of acetamiprid concentration and $\Delta I/I_0$. (**C**) The response current of the biosensor incubated with different concentrations of acetamiprid towards 0.1 mM $H_2O_2$; (**D**) the relationship between acetamiprid concentration incubated by biosensor and $\Delta I$. The inner illustration showed the linear relationship between logarithm of acetamiprid concentration and $\Delta I$. a–h represent the concentration of acetamiprid from 0, $10^{-12}$, to $10^{-6}$ g mL.$^{-1}$

## The specificity and stability of the aptasensor

To evaluate the selectivity of the dual-mode biosensor, several kinds of pesticides and inorganic salts were used as the possible interferences, such as maltose, ascorbic acid, saccharose, citric acid, chlorpyrifos, methyl parathion, fenitrothion, azathioprine, parathion-methyl, fenitrothion, urea, glucose, carbofuran, KCl, $NaNO_2$, and $CuSO_4$. As shown in Fig. 5A, the interference studies were estimated at the optimum conditions in 1.0 μM acetamiprid solution and various concentrations of the interference species. The tolerance limit concentration was considered the concentration of the interference species which offered an error of less than 5% in the measurement of acetamiprid [35, 36]. As shown in Fig. 5A and B, 500-fold of KCl, $NaNO_2$, $CuSO_4$, maltose, ascorbic acid, saccharose, citric acid, urea, and glucose; 200-fold of chlorpyrifos, methyl parathion, fenitrothion, and azathioprine; 100-fold of parathion-methyl; and 20-fold of fenitrothion and carbofuran did not cause no obvious interference in the determination process of acetamiprid. These results indicated that the dual-mode biosensor possessed the excellent selectivity for acetamiprid.

**Table 1** Analytical performance of acetamiprid detection platforms

| Sensing platform | Detection technique | Detection limit/M | Linear range/M | Reference |
|---|---|---|---|---|
| Nitrogen-doped graphene | DPV | $0.15\times10^{-9}$ | $5.0\times10^{-10}$ to $7.8\times10^{-6}$ | [28] |
| Au-rGO | DPV | $2.9\times10^{-15}$ | $0.1\times10^{-12}$ to $10.0\times10^{-9}$ | [29] |
| Gold nanoparticles | DPV | $0.086\times10^{-6}$ | $0.25\times10^{-6}$ to $2.0\times10^{-6}$ | [30] |
| rGO-AgNPs/PB-AuNPs | CV | $0.3\times10^{-12}$ | $1\times10^{-12}$ to $1\times10^{-6}$ | [31] |
| Au-TAN | ECL | $0.0576\times10^{-12}$ | $0.1\times10^{-12}$ to $10\times10^{-9}$ | [32] |
| cDNA-UCNPs | Fluorescence | $0.65\times10^{-6}$ | $4.0\times10^{-9}$ to $5.1\times10^{-7}$ | [33] |
| MWCNTs/rGONRs | Photoelectron-chemical | $0.2\times10^{-12}$ | $0.5\times10^{-12}$ to $10\times10^{-6}$ | [34] |
| PEDOT/CQDs/PB | DPV<br>I-T | $3.1\times10^{-15}$<br>$2.3\times10^{-15}$ | $4.5\times10^{-15}$ to $4.5\times10^{-9}$<br>$4.5\times10^{-15}$ to $4.5\times10^{-9}$ | This work |

*rGO*, reduced graphene oxide; *AgNPs*, silver nanoparticles; *PB*, Prussian blue; *AuNPs*, gold nanoparticles; *TAN*, tetrahedral aptamer nanostructure; *cDNA-UCNPs*, complementary DNA-conjugated upconversion nanoparticles; *CQDs*, carbon quantum dots; *MWCNTs/rGONRs*, MWCNTs/reduced graphene oxide nanoribbons

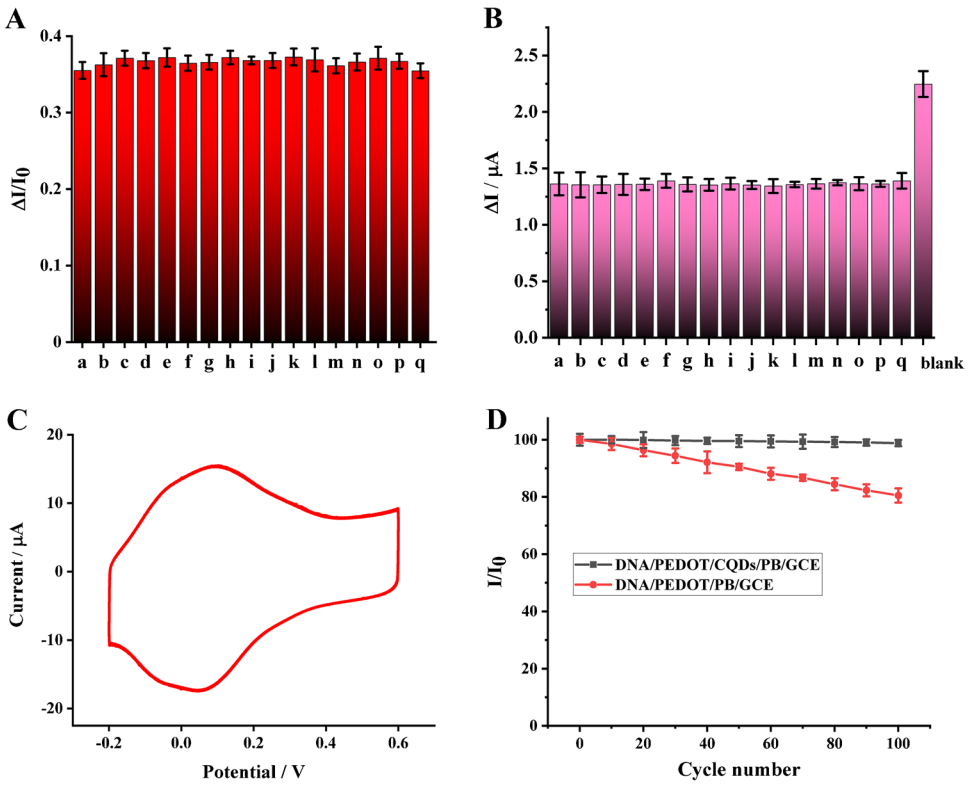


**Fig. 5** (**A** and **B**) The interference tests using dual-mode biosensor towards the mixture of maltose (a), ascorbic acid (b), saccharose (c), citric acid (d), chlorpyrifos (e), methyl parathion (f), fenitrothion (g), azathioprine (h), parathion-methyl (i), fenitrothion (j), urea (k), glucose (l), carbofuran (m), KCl (n), $NaNO_2$ (o), $CuSO_4$ (p) and acetamiprid, and only acetamiprid (q). (**C**) CV curves of 50 circles by the biosensor in a PBS (pH 4.0). (**D**) Oxidation peak current changes of DNA/PEDOT/CQDs/PB/GCE (a) and DNA/PEDOT/PB/GCE (b) at different cycle numbers

Moreover, 50 cycles of CV curves of the biosensors were recorded in PBS (pH 4.0). The DNA/PEDOT/CQDs/PB/GCE was able to retain 98.8% of its initial value of oxidation peak current after 50 cycles, while the DNA/PEDOT/PB/GCE just retained 80.1% (Fig. 5C and D). These results clearly indicated that the DNA/PEDOT/CQDs/PB/GCE had excellent stability.

## Real sample analysis

The dual-mode biosensor was used to detect acetamiprid pesticide in Chinese cabbage cultivated in our laboratory to verify the possibility of practical application. Different concentrations of acetamiprid were added into 100-fold diluted Chinese cabbage extract to perform the validation procedure. For the DPV mode (Figure S8), the linear equation ($\Delta I/I_0 = 0.05573 \log C + 0.7123$, $R^2 = 0.998$) was obtained with the acetamiprid concentration range from $10^{-12}$ to $10^{-6}$ g $mL^{-1}$. It was found that the slope of the linear curve obtained in PBS and vegetable juice was close, which proved that the biosensor had good selectivity and robustness. Moreover, to further confirm the practical application of the dual-mode strategy in the assay of acetamiprid, the HPLC technique was used to detect acetamiprid in vegetable extract according to the previous report [37]. As shown in Table 2, the coincidence rate (DPV/I-T) between the detection results fell between 91.5 and 100%. The detection results of HPLC were basically consistent with the dual-mode detection results. The detection limit of the dual-mode biosensor for vegetables was $6.84 \times 10^{-7}$ mg $L^{-1}$ and $4.99 \times 10^{-7}$ mg $L^{-1}$ (DPV and I-T modes). According to the current GB 2763–2016 in China, the maximum

**Table 2** Determination of acetamiprid in vegetable samples ($n = 3$)

| Sample | HPCL method (μg $mL^{-1}$) | | Sample | Biosensor method (ng $mL^{-1}$) | | | | |
|---|---|---|---|---|---|---|---|---|
| | Detected | RSD (%) | | Detected by DPV | RSD | Detected by I-T | RSD (%) | Coincidence rate (DPV/I-T) (%) |
| 1 | 0.045 | 5.6 | 1′ | 0.043 | 5.1 | 0.047 | 3.2 | 91.5 |
| 2 | 0.094 | 1.6 | 2′ | 0.089 | 3.8 | 0.096 | 2.5 | 92.7 |
| 3 | 0.47 | 2.1 | 3′ | 0.045 | 2.9 | 0.045 | 1.7 | 100 |
| 4 | 0.97 | 1.0 | 4′ | 0.094 | 4.1 | 0.095 | 2.4 | 98.9 |

RSD (%) ($n = 3$), 1′, 2′, 3′, and 4′ samples were obtained by diluting 1, 2, 3, and 4 samples 1000 times

residue limits of acetamiprid in vegetables are 1.0 mg $L^{-1}$. Therefore, the dual-mode biosensor could meet the requirement for the quantitative detection of residual acetamiprid in vegetables.

At the same time, it was noted that when this method was applied to the detection of pesticide residues in actual samples, vegetable samples need to be processed cumbersome. It is expected that further developed detection methods could realize the direct detection of samples without pretreatment.

## Conclusion

A dual-mode (DPV and I-T) biosensor based on PEDOT/CQDs/PB has been constructed for the detection of acetamiprid. Within the designed assaying system, PB provided a sensitive electrochemical signal, and PEDOT/CQDs/PB with good catalytic ability for hydrogen peroxide produced a significantly enhanced current signal. These unique sensing performances, such as high sensitivity, wide linear range, and low detection limit, made this assay a very practical method for the detection of pesticide residues in actual samples. It is expected that the dual-mode strategy for the development of biosensor may open perspectives towards the construction of new biosensors with high sensitivity, accuracy, and selectivity.

**Supplementary Information** The online version contains supplementary material available at https://doi.org/10.1007/s00604-022-05434-y.

**Funding** This work was funded by the National Natural Science Foundation of China (21705088), Shandong Provincial Key R&D Plan (Major Scientific and Technological Innovation Project) (2022CXGC010611, 2022CXGC010401), and Shandong Provincial Peanut Industry Technology System Project (SDAIT-04–09).

## Declarations

**Conflict of interest** The authors declare no competing interests.

## References

1. Li H, Qiao Y, Li J, Fang H, Fan D, Wang W (2016) A sensitive and label-free photoelectrochemical aptasensor using Co-doped ZnO diluted magnetic semiconductor nanoparticles. Biosens Bioelectron 77(77):378–384
2. Balsebre A, Baez ME, Martinez J, Fuentes E (2018) Matrix solid-phase dispersion associated to gas chromatography for the assessment in honey bee of a group of pesticides of concern in the apicultural field. J Chromatogr A 1567:47–54
3. Hirotaka O, Msahiro O, Kazuhiko A, Yoko K, Shinjiro H (2002) Determination of acetamiprid, imidacloprid, and nitenpyram residues in vegetables and fruits by high-performance liquid chromatography with diode-array detection. J Agr Food Chem 50(16):4464–4467
4. Faraji M, Noorbakhsh R, Shafieyan H, Ramezani M (2018) Determination of acetamiprid, imidacloprid, and spirotetramat and their relevant metabolites in pistachio using modified QuEChERS combined with liquid chromatography-tandem mass spectrometry. Food Chem 240:634–641
5. Bera MK, Behera L, Mohapatra S (2021) A fluorescence turn-down-up detection of Cu2+ and pesticide quinalphos using carbon quantum dot integrated UiO-66-NH2. Colloids Surf A 624(2021):126792
6. Vasilescu A, Marty J (2016) Electrochemical aptasensors for the assessment of food quality and safety. TrAC Trends Anal Chem 11(024):60–70
7. Kong X, Zhang B, Wang J (2021) Multiple roles of mesoporous silica in safe pesticide application by nanotechnology: a review. J Agric Food Chem 69(2021):6735–6754
8. Lu H, Wang H, Yang L, Zhou Y, Xu L, Hui N, Wang D (2021) A sensitive electrochemical sensor based on metal cobalt wrapped conducting polymer polypyrrole nanocone arrays for the assay of nitrite. Microchim Acta 189(1):26
9. Hui N, Wang J, Wang D, Wang P, Luo X, Lv S (2022) An ultrasensitive biosensor for prostate specific antigen detection in complex serum based on functional signal amplifier and designed peptides with both antifouling and recognizing capabilities. Biosens Bioelectron 200:113921
10. Li Y, Li Y, Hong M, Bin Q, Lin Z, Lin Z, Cai Z, Chen G (2013) Highly sensitive protein molecularly imprinted electrochemical sensor based on gold microdendrites electrode and prussian blue mediatedamplification. Biosens Bioelectron 42C(Complete):612–617
11. Carneiro S V, Queiroz V R, Cr Uz A, Fechine L, Fechine P (2019) Sensing strategy based on carbon quantum dots obtained from riboflavin for the identification of pesticides. Sens Actuators B 301(August):127149
12. Jiang Y, Zhang X, Shan C, Hua S, Zhang Q, Bai X, Dan L, Niu L (2011) Functionalization of graphene with electrodeposited Prussian blue towards amperometric sensing application. Talanta 85(1):76–81
13. Yang L, Wang J, Lü H, Hui N (2021) Electrochemical sensor based on Prussian blue/multi-walled carbon nanotubes functionalized polypyrrole nanowire arrays for hydrogen peroxide and microRNA detection. Microchim Acta 188(1):1–12
14. Wang L, Tricard S, Yue P, Zhao J, Fang J (2016) Polypyrrole and graphene quantum dots @ Prussian Blue hybrid film on graphite felt electrodes: application for amperometric determination of l-cysteine. Biosens Bioelectron 77(2016):1112–1118
15. Su A, No A, Ma B (2021) Enzyme-free detection of hydrogen peroxide with a hybrid transducing system based on sodium carboxymethyl cellulose, poly(3,4-ethylenedioxythiophene) and Prussian blue nanoparticles. Anal Chim Acta 1172(2021):338664
16. Jin E, Lu X, Cui L, Chao D, Wang C (2010) Fabrication of graphene/prussian blue composite nanosheets and their electrocatalytic reduction of $H_2O_2$. Electrochim Acta 55(24):7230–7234
17. Wang L, Ye Y, Lu X, Wu Y, Sun L, Tan H, Xu F, Song Y (2013) Prussian blue nanocubes on nitrobenzene-functionalized reduced graphene oxide and its application for $H_2O_2$ biosensing. Electrochim Acta 114(2013):223–232
18. Wang C, Li Z, Guo Z, Xu J, Wang H, Zhai K, Xin Z (2010) A novel hydrazine electrochemical sensor based on the high specific surface area graphene. Microchim Acta 169(1–2):1–6
19. Xu E, Yang H, Li P, Wang Z, Liu S (2020) Dual-mode detection of PARP-1 by fluorescence and chemiluminescence. Sens Actuators B 330(20):129288

20. Guo CX, Zhao D, Zhao Q, Peng W, Lu X (2014) Na+-functionalized carbon quantum dots: a new draw solute in forward osmosis for seawater desalination. Chem Commun 50(55):7318–7321
21. Hui N, Wang W, Xu G, Luo X (2015) Graphene oxide doped poly(3,4-ethylenedioxythiophene) modified with copper nanoparticles for high performance nonenzymatic sensing of glucose. J Mater Chem B 3(4):556–561
22. Wang J, Wang D, Hui N (2020) A low fouling electrochemical biosensor based on the zwitterionic polypeptide doped conducting polymer PEDOT for breast cancer marker BRCA1 detection. Bioelectrochemistry 136:107595
23. Cao L, Liu Y, Zhang B, Lu L (2010) In situ controllable growth of Prussian blue nanocubes on reduced graphene oxide: facile synthesis and their application as enhanced nanoelectrocatalyst for $H_2O_2$ reduction. ACS Appl Mater Interfaces 2(8):2339–2346
24. Martindale B, Hutton G, Caputo CA, Reisner E (2015) Solar hydrogen production using carbon quantum dots and a molecular nickel catalyst. J Am Chem Soc 137(18):6018–6025
25. He Y, Zhou X, Zhang X, Ma L, Jiang Y, Gao J (2020) Self-reducing Prussian blue onTi3C2Tx MXene nanosheets as a dual-functional nanohybrid for hydrogen peroxide and pesticide sensing. Ind Eng Chem Res 59(35):15556–15564
26. Madrakian T, Maleki S, Gilak S, Afkhami A (2017) Turn-off fluorescence of amino-functionalized carbon quantum dots as effective fluorescent probes for determination of isotretinoin. Sens Actuators B 247(03):428–435
27. Ozeki T, Watanbe I, Ikeda S (1987) Study of the prussian blue/prussian white redox reaction by cyclic voltammothermometry. J Electroanal Chem 236(1–2):209–218
28. Oghli A, Soleymanpour A (2021) Pencil graphite electrode modified with nitrogen-doped graphene and molecular imprinted polyacrylamide/sol-gel as an ultrasensitive electrochemical sensor for the determination of fexofenadine in biological media. Biochem Eng J 167:107920
29. Xue Q, Fang X, Dong T, Pei C, Jian L, Jin G (2019) Ultrasensitive "signal-on" electrochemical aptasensor for assay of acetamiprid residues based on copper-centered metal-organic frameworks. Anal Chim Acta 1050(2018):51–59
30. Rapini R, Cincinelli A, Marrazza G (2016) Acetamiprid multidetection by disposable electrochemical DNA aptasensor. Talanta 161:15–21
31. Xiao S, Jian S, Yao Y, Hui L, Jing H, Ye G (2020) Novel electrochemical aptasensor with dual signal amplification strategy for detection of acetamiprid. Sci Total Environ 705:135905
32. Ye G, Feng Y, Yao Y, Jian L, Shu C, Hao D (2021) Novel Au-tetrahedral aptamer nanostructure for the electrochemiluminescence detection of acetamiprid. J Hazard Mater 401:123794
33. Na S, Yuan D, Zhe T, Hongjie Y, Xiu H, Ming W (2018) Development of an upconversion fluorescence DNA probe for the detection of acetamiprid by magnetic nanoparticles separation. Food Chem 258:289–294
34. Qian L, Juan H, Xiao D, Jing Q, Nan H, Tian Y, Han M, Kun W (2016) Resonance energy transfer from CdTe quantum dots to gold nanorods using MWCNTs/rGO nanoribbons as efficient signal amplifier for fabricating visible-light-driven "on-off-on" photoelectrochemical acetamiprid aptasensor. Sens Actuators, B 235:647–654
35. Hassan OA, Soleymanpour, (2021) Pencil graphite electrode modified with nitrogen-doped graphene and molecular imprinted polyacrylamide/sol-gel as an ultrasensitive electrochemical sensor for the determination of fexofenadine in biological media. Biochem Eng J 167:107920
36. Rouhani M, Soleymanpour, (2020) Preparation of Dawson heteropolyacid-embedded silver nanoparticles/graphene oxide nanocomposite thin film used to modify pencil graphite electrode as a sensor for trace electrochemical sensing of levodopa. Mater Sci Eng C 117:111287
37. Tang X, Li X, Ma D, Lu L, Qu B (2018) A label-free triplex-to-G-qadruplex molecular switch for sensitive fluorescent detection of acetamiprid. Talanta 025(18):30717–30713